express
polymer letters

Research article

In situ catalyzed poly(ε-caprolactone)/organic rectorite nanocomposites with excellent electrochemical performance

*Limin You, Shifan Zhang, Zhuoxiong Huang, Wanle Pi, Jiaqi Liu, Rui Ma**

Faculty of Materials Science and Chemistry, China University of Geosciences, 430074 Wuhan, China

Abstract. In recent years, solid polymer electrolytes (SPE) has attracted much attention because of its good safety and environmental stability, among which poly(ε-caprolactone) (PCL) based solid electrolyte film is one of the most potential materials. We have adopted the method of synthesizing polymer nanocomposites with natural clay, which can effectively meet the needs of electrolytes. In this study, cetyl trimethyl ammonium bromide (CTAB) was used to modify rectorite (REC), and the ε-CL monomer is inserted between the rectorite silicate layers. PCL/organic rectorite (OREC) nanocomposites were synthesized by *in situ* intercalation polymerization. The yield of the polymer nanocomposite could reach 93.6% when the molecular weight of the polymer nanocomposite was 39 000. The effects of OREC addition on the morphology, thermal stability, and electrochemical properties of PCL/OREC nanocomposites were investigated by various characterization methods. The temperature can be increased by 50 °C when the thermal decomposition is 50 wt%, and the crystallinity decreases by 4.6%. Composite polymerelectrolytes (CPEs) (PCL/OREC) showed a good electrical conductivity of $1.13 \cdot 10^{-4}$ S·cm^{-1} at 60 °C and an excellent capacity retention rate of 96.7% after 100 cycles at 0.5 C current density. This study has important guiding significance for the development of polymer nanocomposites as solid electrolytes.

Keywords: biopolymer, ring-opening polymerization, electrical property, poly(caprolactone), clay

1. Introduction

Poly(ε-caprolactone) (PCL) is a synthetic biodegradable polyester that is compatible with a variety of polymers and is one of the most promising biodegradable polymers in the market at present [1]. Moreover, due to the unique lithium-ion complexation and transport mechanism, PCL-based solid polymer electrolyte (SPE) has a wide electrochemical stability window and high lithium ion migration number [2–5], so PCL can be applied to the preparation of SPE. However, the poor thermal stability and semi-crystallinity of PCL [6] limit the cell cycle performance and ionic conductivity of PCL-based solid electrolytes. The addition of organic layered silicates as nanoparticles to PCL can ameliorate these limitations. However, the compatibility and dispersion of natural mineral materials in polymers are poor. If the

traditional physical blending method is used to prepare polymer composite materials, uneven dispersion may occur in silicate mineral polymer materials, and poor compatibility leads to the reduction of mechanical and thermal properties of composite materials [7]. And the presence of larger mineral particles in the polymer matrix creates a lot of 'Blocks' which in part blocks the movement of ions, resulting in lower conductivity. In order to overcome these difficulties, the method of *in situ* intercalation polymerization is adopted. By *in situ* polymerization of monomers between layers, the silicate layer is stripped, and the large particle size is converted to a smaller size and distributed uniformly in the polymer matrix. As Ilsouk *et al.* [8] prepared poly(ε-caprolactone)/organomodified Moroccan beidellite clay through *in situ* polymerization, Moroccan beidellite

---

clay was well stripped and dispersed in PCL, which is consistent with other relevant reports [9–11]. In addition to improving the thermal stability of polymer, the addition of nano-sized particles enhanced the activity of polymer molecular chains, thus improving the ionic conductivity of polymer electrolytes. Due to the nano-dispersion of the silicate layer, the properties of ordinary materials are completely different from those of composite materials with inorganic components dispersed at the micron level. Unexpected properties were observed, such as large increases in thermal stability, mechanical strength, and permeability to gases such as oxygen and water [12, 13].

Compared with silicate minerals such as montmorillonite and kaolin, there is relatively little research on rectorite nanocomposites, so there is potential for research and development. Natural rectorite is a special layered silicate mineral composed of octahedral mica and octahedral montmorillonite layers stacked in a 1:1 ratio, with good colloid properties and cation exchange capacity [14, 15]. Because of the special layered structure, it has the characteristics of both mica and montmorillonite [16]. Recently, rectorite (REC) has been widely used in polymer modification. It was found that the mechanical and thermal properties of the polymer were greatly enhanced with the introduction of REC [17]. In addition, rectorite is more resistant to heat and is a better barrier than montmorillonite because of its higher aspect ratio [18].

Considering the dual advantages of excellent cation exchange and the low cost of REC, cetyl trimethyl ammonium bromide (CTAB) was used to modify rectorite to obtain organic rectorite (OREC). PCL/OREC nanocomposites were synthesized by intercalating ε-CL monomer into OREC layers and *in situ* intercalation polymerization. The optimum synthesis conditions of PCL/OREC nanocomposites were studied by changing the ratio of initiator to OREC. The effects of OREC incorporation on the morphology, thermal stability, and electrochemical properties of PCL/OREC nanocomposites were investigated by various characterization methods.

2. Experimental
2.1. Materials
Ca-Rectorite (Ca-REC) (95% purity) was purchased from Lingshou Country Deheng Mineral Products Co., Ltd (Hebei, China). Hexadecyl trimethyl ammonium bromide (CTAB, 99% purity) was purchased from Shanghai Aladdin Bio-Chem Technology Co., Ltd (Shanghai, China). Tin 2-ethylhexanoate ($Sn(Oct)_2$, 98% purity) was purchased from Shanghai Macklin Biochemical Co., Ltd. (Shanghai, China). Methanol, dichloromethane, hydrochloric acid and Al_2O_3 (99.9% metals basis, α-phase, 30 nm, 99% purity) were purchased from Sinopharm Chemical Reagent Co., Ltd (Shanghai, China). ε-caprolactone (ε-CL, 99% purity) was purchased from Shanghai Aladdin Bio-Chem Technology Co., Ltd (Shanghai, China).

2.2. Purification of rectorite
10 g REC was added to 100 ml deionized water and stirred to a uniform liquid phase, then 3 g sodium hexametaphosphate was added as dispersant and stirred at room temperature for 5 h. The solution was poured into the centrifugal tube and the upper solid was collected after high-speed centrifugation; the lower black solid was removed as impurities, and then an appropriate amount of deionized water was added for washing. This process was repeated three times. After drying and grinding, purified REC is stored in a dry environment.

2.3. Organization of rectorite
REC was added to 1 mol/l hydrochloric acid solution with a solid-liquid ratio of 1:20. Disperse for 15 min with ultrasound and stir for 12 h. The solution was poured into a centrifuge tube and washed three times until the pH value approached 7. After drying for 12 h at 80 °C, the acid REC was obtained by grinding. 5 g acidified REC was added to 50 ml deionized water, stirred evenly, and 0.879 g CTAB was added. The reaction was performed at 60 °C for 5 h under a nitrogen atmosphere, followed by high-speed centrifugation and deionized water washing for three times. The supernatant was taken, and no bromine ions were detected with silver nitrate solution, dried at 80 °C for 12 h, and OREC was obtained by grinding.

2.4. Synthesis of PCL/OREC nanocomposites
PCL/OREC nanocomposites were prepared by monomer intercalation *in situ* polymerization. A certain amount of ε-CL and OREC was added to the branching flask, and the samples were dispersed by ultrasonic for 30 min in a nitrogen atmosphere and stirred at 66 °C for 12 h. A certain amount of $Sn(Oct)_2$ was added to the system as a catalyst, and
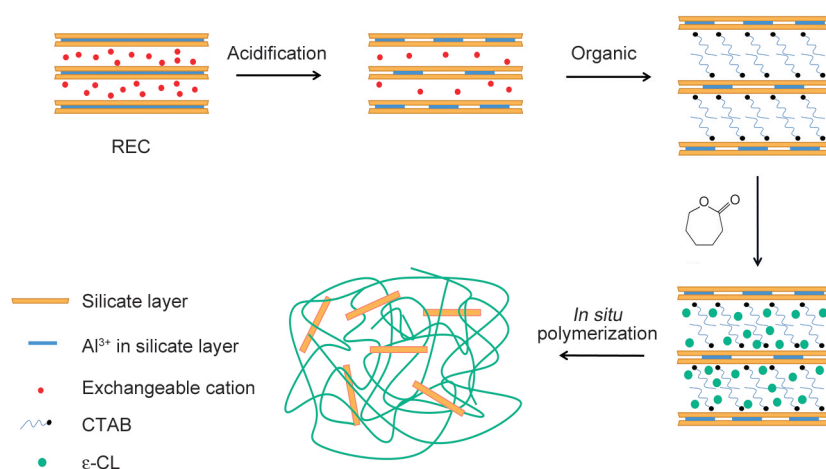
Figure 1. Mechanism of PCL/OREC synthesis.

the flask was stirred in an oil bath at 140 °C for 24 h after being purged with nitrogen three times. At the end of the reaction, an appropriate amount of methylene chloride was added to the system to dissolve the product. When the product was completely dissolved, excessive methanol was added and placed in the refrigerator overnight. After the product is precipitated from the solution, it is washed and filtered with methanol to remove unreacted monomers and catalysts. The product was dried at a vacuum of 40 °C for 48 h, then weighed and yield calculated. The general procedure is illustrated in Figure 1.

2.5. Synthesis of composite polymer electrolytes (CPEs)

In the glove box, an appropriate amount of pure PCL or PCL/OREC nanocomposites and LiTFSI were dissolved in an appropriate amount of dimethyl carbonate, in which LiTFSI accounted for 20% of the mass of the polymer and stirred at 60 °C for 1 h. Then 15 wt% Al_2O_3 powder was added and stirred for a certain time under continuous heating. When the system was completely evenly dispersed, the solution was poured onto a glass plate with a spatula to form a film and dried at room temperature for 24 h to remove residual solvents. The resulting CPE film was cut into 19 mm diameter disks and assembled into coin-shaped cells in a glove box.

2.6. Characterization

The phase and composition of the samples were characterized by X-ray powder diffraction (XRD, Bruker D8 Advance, Bruker AG, Saarbrucken, Germany) using Cu K_α radiation ($\lambda = 0.15406$ nm) and characterized by Fourier transform infrared

spectrometer (FTIR, ThermoFisher Nicolet iS50, Thermo Fisher Scientific, Massachusetts, USA). Thermal analysis was performed in nitrogen at a heating rate of 10 °C·min⁻¹ from 30 to 600 °C (TG, Netzsch STA 2500, Netzsch, Selbu, Germany). The morphology and structure were examined by scanning electron microscopy (SEM, Hitachi SU8010, Hitachi Corporation, Tokyo, Japan and GeminiSEM 300, Carl Zeiss AG, Oberkochen, Germany). The thermal behavior of the samples was performed by differential scanning calorimetry (DSC, Discovery DSC 25, TA Instruments, Newcastle, USA). Firstly, the samples were heated from ambient to 80 °C at a heating rate of 20 °C·min⁻¹ and held isothermally at 80 °C for 10 min; secondly, the samples were cooled from 80 to –80 °C at a cooling rate of 20 °C·min⁻¹ and held isothermally for 10 min; and finally, the samples were again heated from –80 to 80 °C at a heating rate of 20 °C·min⁻¹. The chemical structures of the samples were recorded by nuclear magnetic resonance (¹H-NMR, Bruker 400M, Bruker AG, Saarbrucken, Germany). The number-average molecular weight (M_n) of the samples was determined using gel permeation chromatography (GPC, Breeze 2 Hplc 1525, Waters Corporation, Massachusetts, USA). The dynamic thermomechanical analyzer (DMA) was used, and the test conditions were as follows: using a single cantilever fixture, the test temperature range was –120 to 30 °C, the test frequency was 1 Hz, and the heating rate was 2 °C·min⁻¹ (Discovery DMA850, TA Instruments, Newcastle, USA). The ionic conductivities of the membranes were determined by electrochemical impedance spectroscopy (EIS, Zennium X, Zana Electrochemistry, Kronach, Germany). The charge and discharge tests

were performed from the LAND system (LAND, CT2001A, Wuhan Shenglan Electronic Technology Co., Wuhan, China). For cycling performance, the cells were charged and discharged with a 0.5 C rate.

3. Results and discussion
3.1. Structural analysis of REC and OREC
FTIR spectra of REC and OREC are shown in Figure 2. In the FTIR spectra of REC, the peak at 3620 cm^{-1} was related to the tensile vibration of the hydroxyl group of the Al–OH unit in rectorite. The peak values of 3419 and 1637 cm^{-1} are correlated with H–O–H tensile vibration and bending vibration of H_2O [19]. The peak at 1050 cm^{-1} is attributed to Si–O–Si tensile vibration in the plane. A peak of 822 cm^{-1} was associated with the bending vibration of Si–O–Al, while the peak of 822 cm^{-1} disappeared in FTIR spectra of acid-treated OREC. These results showed that the strength of the Si–O–Al band was weakened after acid treatment, and part of Al^{3+} in the surface skeleton was dissolved. Meanwhile, it was further indicated that acid treatment could change the surface properties of rectorite without destroying the structure of the original rectorite [20, 21], which was consistent with other layered silicate minerals with similar structures, such as montmorillonite and talc [22, 23]. In the FTIR spectrum of OREC, the broad peak at 3590 cm^{-1} and the peak at 1637 cm^{-1} were attributed to the tensile vibration and bending vibration of adsorbed water molecules. Compared with the vibration peak at 1050 cm^{-1} in the REC spectrum, the OREC spectrum moves to a higher wave number of 1100 cm^{-1}, corresponding to the out-of-plane Si–O–Si tensile vibration after acid treatment [24, 25]. At peak

values of 2927, 2852, and 1454 cm^{-1}, they were correlated with characteristic peaks of alkyl chains of surfactants, indicating [26] CTAB molecules were successfully grafted onto the surface of REC.

Figure 3 shows the X-ray diffraction data for REC and OREC. The interlayer distance of rectorite was obtained from the peak position (d_{001}-reflection) of X-ray diffraction data. In the X-ray diffraction data of REC, the d_{001}-reflection of phyllosilicate at $2\theta = 7.20°$ corresponds to the interlayer distance of 12.3 Å. In the X-ray diffraction data of OREC, the d_{001}-reflection of phyllosilicate at $2\theta = 4.98°$ corresponds to the interlayer distance of 17.7 Å. These data show that the d_{001} crystal plane spacing of rectorite increases by 5.4 Å interlayer distance after organic treatment. Cetyltrimethyl ammonium bromide (CTAB) has a long alkyl chain structure and enters the silicate layer through ion exchange with REC [27]. Cationic surfactants can effectively increase the interlayer spacing of clay, thereby effectively reducing the interaction force between clay sheets [28] and improving the compatibility between natural clay and polymer.

The surface morphologies of REC and OREC were characterized by SEM images. It can be observed from Figure 4a that there is uneven particle size in the original REC, and the particle surface is rough, presenting a jagged and irregular sheet structure. As the layers are closely superimposed on top of each other, the spacing between the layers is almost indistinguishable. However, in the SEM image of OREC (Figure 4b), the particle size becomes smaller, the size distribution becomes uniform, more pore structures appear, the layered structure becomes loose,
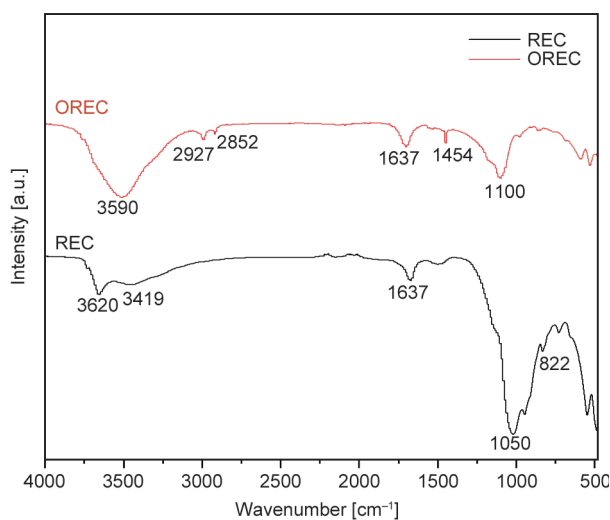
Figure 2. FTIR spectra of REC and OREC.
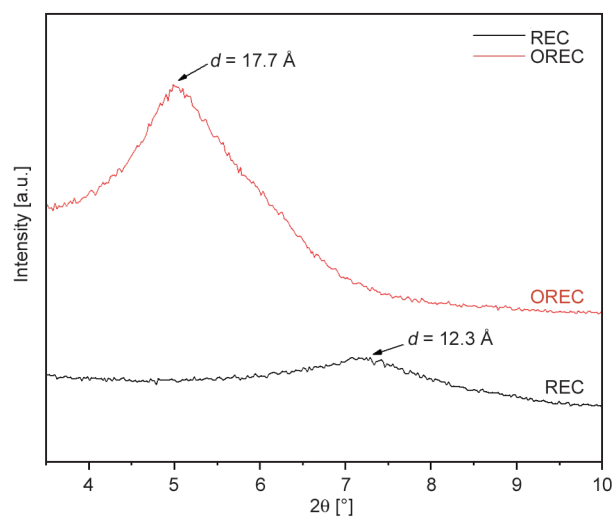
Figure 3. X-ray diffraction patterns of REC and OREC.
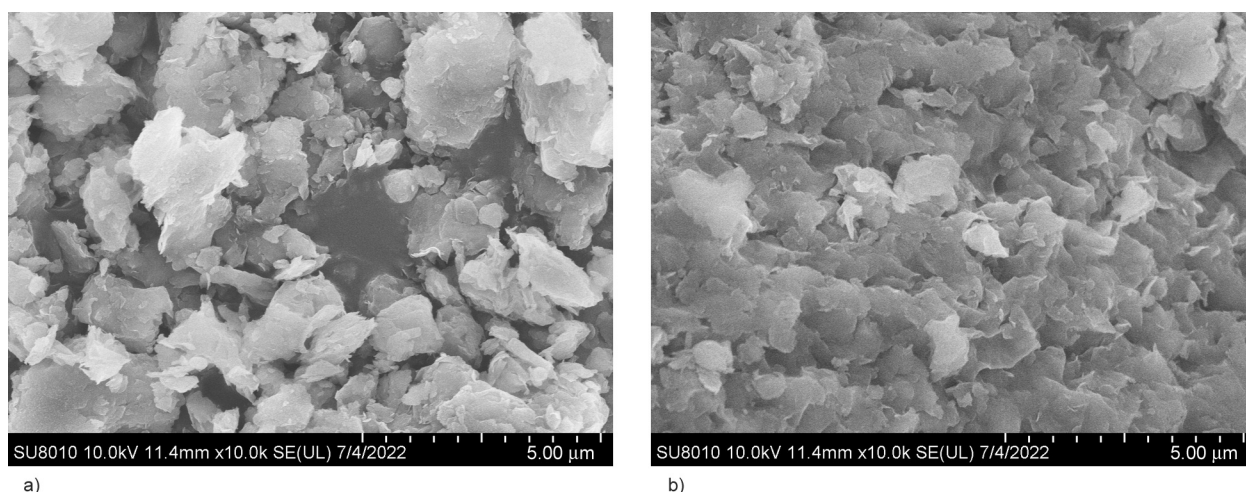
Figure 4. SEM images of a) REC and b) OREC.

and the layered stepped structure can be clearly seen. The results showed that after acid treatment and organic modification, the interlayer spacing increased and became more conducive to monomer entry. This result is consistent with the analysis of XRD.

3.2. Characterization of PCL/OREC nanocomposites

Figure 5 shows the NMR hydrogen spectrum, and the analysis reveals the chemical structure of the sample. ^{1}H-NMR (CDCl$_3$, δ [ppm]):2.2 (H$_a$, 2H), 1.7 (H$_b$, 4H), 1.4(H$_c$, 2H), 4.1 (H$_d$, 2H). The results confirm the successful synthesis of PCL [29].

To study the optimum ratio of initiator Sn(Oct)$_2$ and OREC in the polymerization of ε-CL. Table 1 shows the effects of different initiator/monomer (I/M) mass ratios on the conversion rate and polymer dispersion index PDI (M_w/M_n) of nanocomposites when OREC addition amounts are 1, 2 and 4 wt%, respectively. As
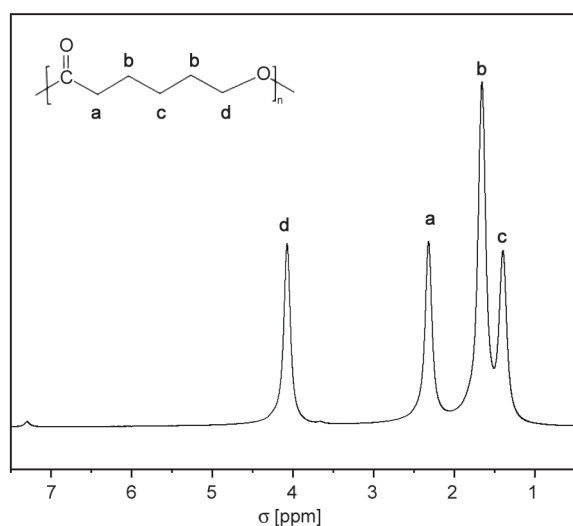
Figure 5. NMR hydrogen spectrum of PCL.

can be seen from the above table, the best conditions for composite synthesis are OREC with $I/M = 0.2$ and 2 wt%. Therefore, the subsequent tests were carried out with this sample.

When OREC content was increased to 2 wt%, a decrease in polymer dispersion index was observed. This is because the chain growth in the clay layer is limited at the beginning of polymerization, and these chains are not easy to participate in the transesterification reaction. When the chain grows long enough to achieve the effect of stripping, this protection will disappear [30]. The dispersion of rectorite in PCL was greatly improved after the stripping effect occurred, and the inorganic/organic interface effect was enhanced. After acid treatment, some Si–O–Al structures in rectorite are dissolved, resulting in the formation of more Si–OH. These surface hydroxyl groups can attack the C–O bond in the caprolactone monomer and achieve the purpose of ring-opening polymerization [31]. Therefore, a portion of the PCL molecular chain grows on the surface of the REC; we believe that rectorite and

Table 1. Effect of different ratios on conversion, molecular weight, and PDI of polymer nanocomposites.

Sample	OREC [%]	I/M [wt%]	CR [%]	M_n [g·mol^{-1}]	PDI
1	1	0.1	89.60	32 000	1.65
2	1	0.2	88.00	36 000	1.61
3	1	0.4	86.50	35 000	1.84
4	2	0.1	89.20	34 000	1.39
5	2	0.2	93.60	39 000	1.23
6	2	0.4	95.60	35 000	1.50
7	4	0.1	89.40	19 000	1.61
8	4	0.2	94.40	22 000	1.58
9	4	0.4	92.00	20 000	1.78

Sn(Oct)$_2$ cooperate to catalyze ε-CL polymerization. When the clay concentration reached 4 wt%, clay stripping became difficult and resulted in shorter molecular chain growth lengths and lower molecular weight of polymers. At these concentrations, stripped and unstripped rectorite co-existed in the composite, leading to an increase in PDI.

Figure 6 shows the X-ray diffraction data of PCL with different amounts of rectorite. It can be observed that the diffraction peak of the d_{001} crystal plane of rectorite exists in PCL with a mass fraction of OREC of 4 wt%, which indicates that part of rectorite is not stripped when the amount of rectorite is too large. However, when a low amount of rectorite was added, no d_{001} crystal plane was observed, indicating that the interlayer distance became infinite and rectorite was completely stripped and dispersed in PCL. At the same time, the peak width of 1%OREC to 4%OREC is significantly different. With the increase of OREC addition, the peak width of PCL/OREC XRD curve is wider, and the peak height is lower, indicating that the presence of
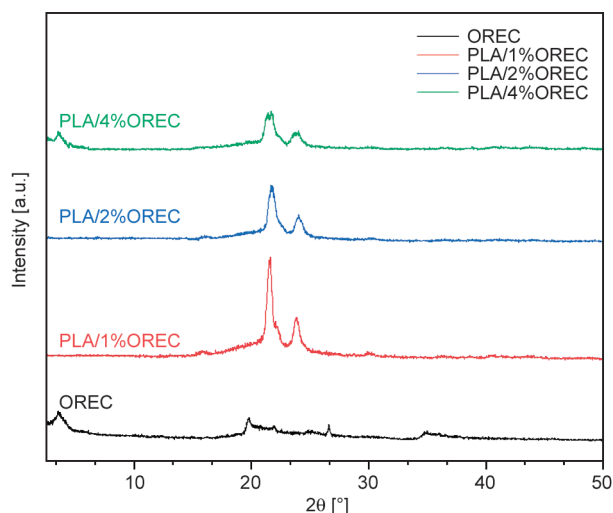
Figure 6. X-ray diffraction data of PCL with different amounts of rectorite.

OREC can reduce the crystallinity of PCL, and the crystallinity of PCL/OREC is lower with the increase of OREC addition.

Figure 7 shows SEM images of pure PCL and PCL/OREC with different OREC content, which are
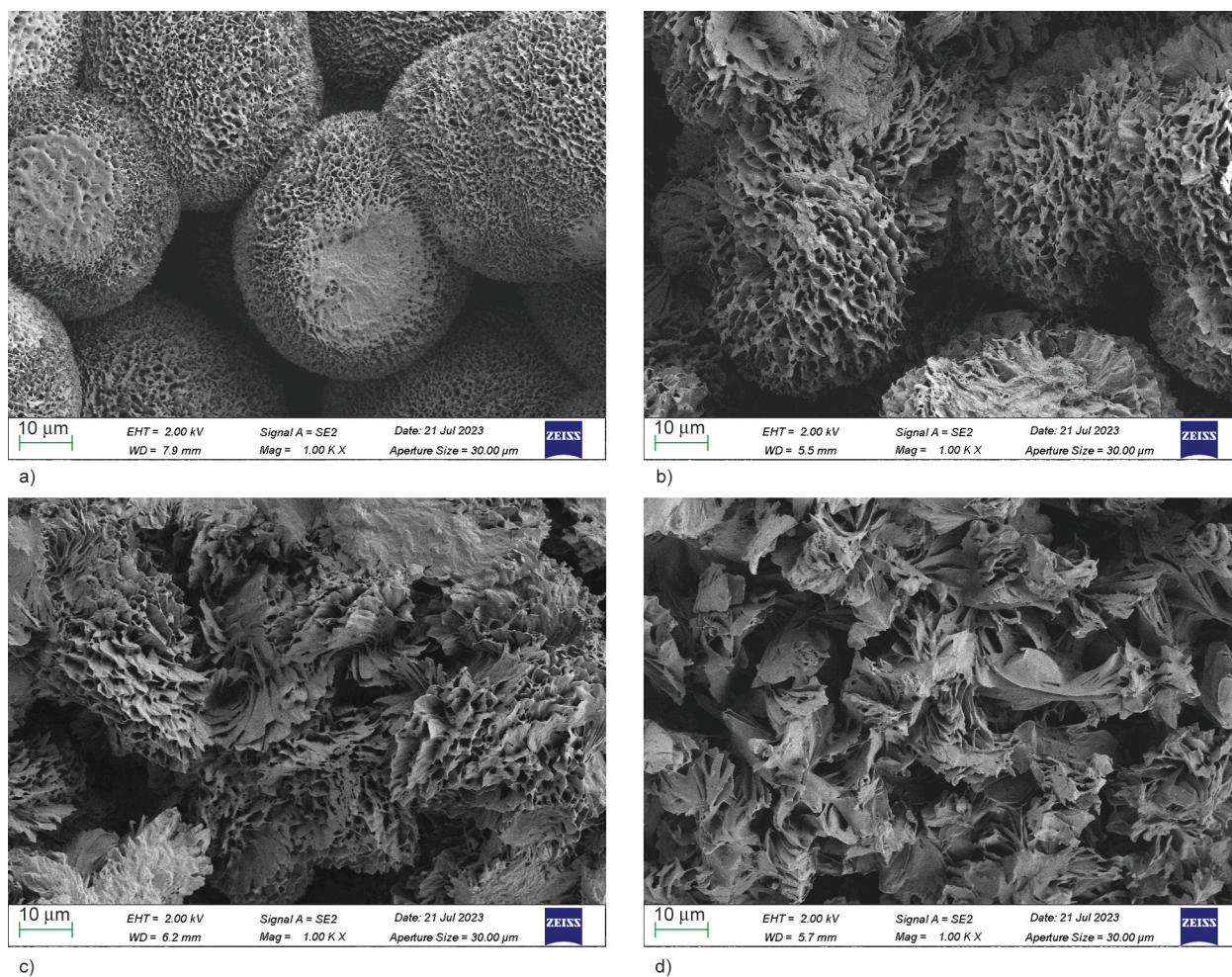
Figure 7. SEM images of a) pure PCL, b) PCL/1%OREC, c) PCL/2%OREC and d) PCL/4%OREC.

sectional images obtained by brittle fracture after liquid nitrogen cooling. As can be seen from Figure 7a, pure PCL shows a well-organized and well-grown spherulite structure, while dispersed rectorite exists in PCL/OREC, and the mobility of the chain is limited, leading to imperfect crystallization, which does not allow the growth of well-developed spherulite structure [32]. It can be seen from Figure 7b–7d that with the increase of OREC content, the spherulite structure in the crystallization process of PCL is gradually weakened, the amorphous region increases and the overall structure becomes loose. This shows that the addition of OREC can inhibit the crystallization of PCL and thus change the polymer structure. Moreover, no mineral was observed, indicating that rectorite completely dispersed in PCL.

Thermogravimetric analysis (TGA) was used to study the thermal degradation behavior of nanocomposites at a heating rate of $10\,°C\cdot min^{-1}$. Figure 8 compares pure PCL with nanocomposites containing 1, 2, and 4 wt% OREC. Compared with pure PCL, the temperature at which the nanocomposite loses 50 wt% increases with the increase of rectorite content and reaches an increase of $50\,°C$ at 4 wt%. This shift to higher temperatures may be due to the barrier properties conferred by the highly anisotropic nanoparticles and the formation of carbon, resulting in reduced permeability/dispersion of oxygen and volatile degradation products through the sample. This indicates that the addition of rectorite can effectively improve the thermal stability of PCL.

Figure 9 shows the DSC curves of different samples. The melting temperature (T_m), melting enthalpy (ΔH_m), and crystallinity (χ_c) data obtained from DSC curves are shown in Table 2. Crystallinity was calculated using the ratio of the heat of melting per gram of sample determined by DSC measurements to the heat of melting corresponding to 100% crystalline PCL ($156\,J\cdot g^{-1}$) [33]. As shown in Table 2, compared with pure PCL, the melting temperature of PCL/OREC nanocomposite basically remains unchanged. However, the melting enthalpy of PCL/OREC decreased with the increase in OREC content, and the crystallinity decreased by 4.6% at 4% OREC. The crystallinity of the PCL/OREC nanocomposite is reduced because the stripped OREC nanoparticles in the nanocomposite limit the mobility of the PCL chain to a certain extent, thereby reducing the crystallinity of the matrix [34, 35]. This is consistent with the results of the previous XRD analysis. In polymers, ionic conduction predominantly occurs in amorphous regions through the local segmental motion [36]. The reduced crystallinity makes the polymer chain segments more flexible, which has a beneficial effect on electrical conductivity [37].

Dynamic mechanical analysis (DMA) is one of the most effective methods to investigate the molecular motion of polymers. It can describe the modulus of

Table 2. The melting temperature (T_m), melting enthalpy (ΔH_m), and crystallinity (χ_c) data of PCL and PCL with different content of OREC.

Sample	T_m [°C]	ΔH_m [J·g⁻¹]	χ_c [%]
Pure PCL	57.6	69.8	44.7
PCL/1%OREC	57.5	67.5	43.3
PCL/2%OREC	57.7	64.6	41.4
PCL/4%OREC	57.3	62.6	40.1

Figure 8. Thermogravimetric analysis of pure PCL and PCL with different content of OREC.
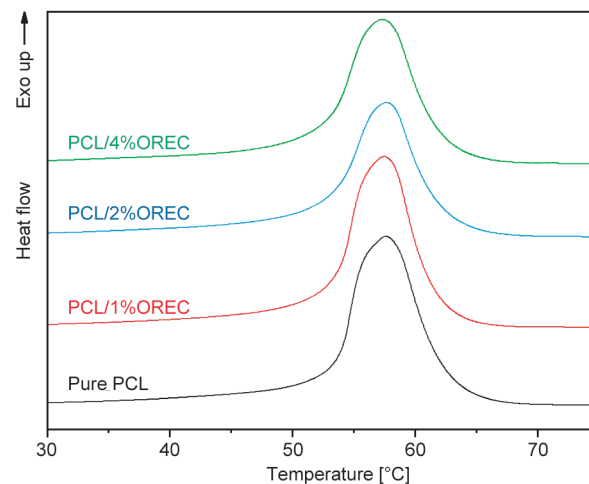
Figure 9. DSC curves of pure PCL and PCL with different content of OREC.
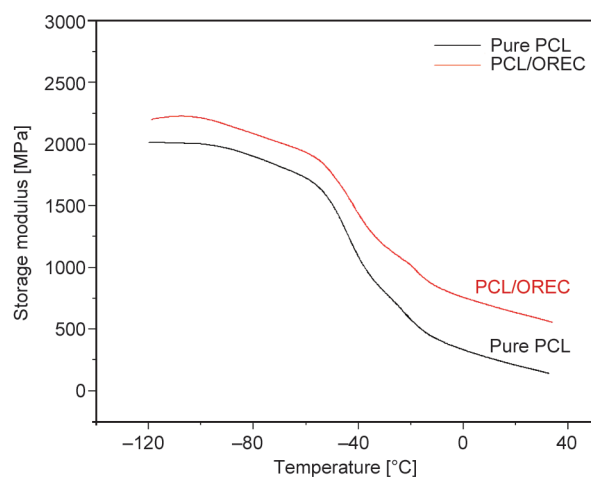
Figure 10. The curve of energy storage modulus of PCL and PCL/OREC.
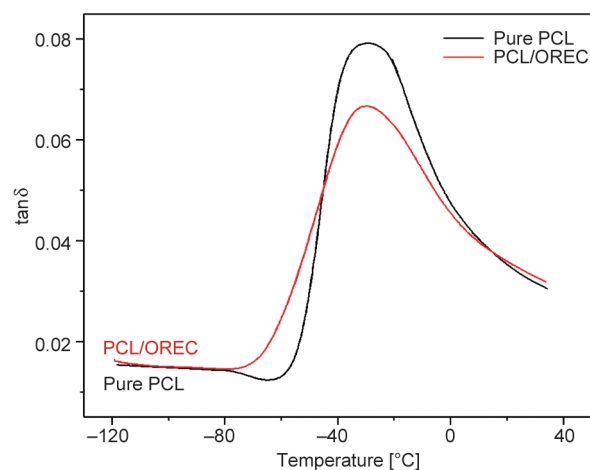
Figure 11. Relationship between temperature and tanδ of PCL and PCL/OREC.

materials, investigate the mechanical internal friction of materials, and explore the molecular motion of various units. The relationship between material microstructure and material properties can be studied. Figure 10 shows the variation curve of energy storage modulus of PCL and PCL/OREC with temperature. As can be seen from the figure, the energy storage modulus of PCL/OREC nanocomposite is higher than pure PCL at different temperatures. The increase in energy storage modulus is due to the uniform dispersion of nanoparticles in the matrix and the strong interaction between nanoparticles and the PCL matrix. The increase of energy storage modulus is beneficial to the practical application of PCL materials at higher temperatures.

As can be seen from Figure 11, the T_α value of PCL/OREC corresponds to –30.5 °C, while that of pure PCL corresponds to –28.1 °C. This phenomenon indicates that the addition of nanoparticles as internal plasticizers increases the distance between polymer molecular chains [38] and reduces the internal friction between polymer chains. Therefore, the degree of interaction between polymer chains decreases, and the T_α value decreases. In addition, compared with pure PCL materials, the maximum value of tan δ of composites with nanoparticles is reduced, mainly because the volume effect caused by the dilution effect after filler is added has a certain effect on the reduction of loss factor. Moreover, there is a strong interaction between the nanoparticles modified by CTAB and the PCL matrix, which can reduce the peak internal friction of the composite [39]. Therefore, the addition of nanoparticles enhances the activity of molecular chains in the system,

thus improving the ionic conductivity of polymer electrolytes.

The ionic conductivity of solid electrolytes is a direct reflection of the ionic conductivity in the material. To obtain ionic conductivity, an AC impedance test is first performed to obtain electrochemical impedance spectroscopy (EIS). Solid electrolyte membrane CPEs (pure PCL and PCL/OREC) was made, and the AC impedance spectrum obtained by testing was shown in Figure 12. The results showed that PCL/OREC samples showed lower ionic resistance compared with pure PCL at temperatures greater than 30 °C. The conductivity values of the samples can be calculated separately, and the results are shown in Table 3. Obviously, in the range of 40 to 60 °C, the conductivity of CPEs (PCL/OREC) is improved compared with that of CPEs (pure PCL). The possible reason is that the addition of inorganic nanoparticles affects the growth pattern of PCL molecular chains, resulting in branched structures that can provide relatively short ion transport paths, reduce the crystallinity of the polymer, and improve the ionic conductivity of the electrolyte. At the same time, uniformly dispersed stripped OREC reduces the intermolecular hydrogen bond strength between the polymer network molecules and increases the proportion of amorphous domains associated with lithium-ion migration, which ultimately improves the ionic conductivity of the sample [40, 41].

The way polymer solid electrolytes transport ions is through the movement of chain segments [42, 43]. The ionic conductivity of pure PCL and PCL/OREC is not much different at room temperature because the chain structure of PCL is relatively static at low
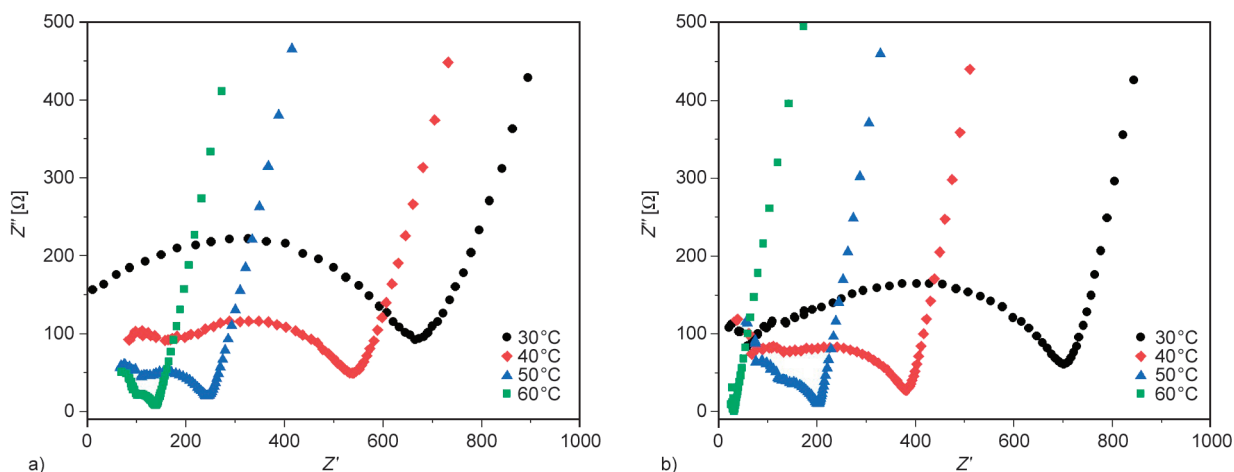
Figure 12. Nyquist plot of a) CPEs (pure PCL) and b) CPEs (PCL/OREC).

Table 3. Ionic conductivity of pure PCL and PCL/OREC at different temperatures.

Sample	Ionic conductivity [S·cm^{-1}]			
	30 °C	40 °C	50 °C	60 °C
CPEs (pure PCL)	$0.56 \cdot 10^{-5}$	$0.73 \cdot 10^{-5}$	$0.16 \cdot 10^{-4}$	$0.27 \cdot 10^{-4}$
CPEs (PCL/OREC)	$0.52 \cdot 10^{-5}$	$0.95 \cdot 10^{-5}$	$0.18 \cdot 10^{-4}$	$1.13 \cdot 10^{-4}$

temperatures, and the activity capacity of PCL and PCL/OREC chains is similar. However, the activity of polymer nanocomposite chains is better at higher temperatures. At the same time, the operating temperature of the battery is generally higher than the normal temperature. At more than 30°C, the chain movement of PCL/OREC is better, lithium ions are easier to transmit, and the ionic conductivity is higher.

LFP//CPE//Li cells were assembled to evaluate the electrochemical performance of the prepared CPEs (PCL/OREC) in lithium solid-state batteries. The experimental temperature is 60 °C, the theoretical specific capacity is set to 170 mAh·g^{-1}, and the test con-

dition of the rate charge and discharge experiment is the current density of 0.5 C. As shown in Figure 13, the discharge capacity shows an upward trend with the increase in the number of cycles, indicating that the activation process of the battery is slow. The reversible discharge capacity is maintained at 181.2 mAh·g^{-1}, and a specific discharge capacity of about 174.2 mAh·g^{-1} was shown after 100 cycles, indicative of good capacity retention at 96.7%.

4. Conclusions

In this paper, the organic rectorite (OREC) was prepared by acid treatment and CTAB modification, and the structural changes of REC before and after modification were obtained by XRD, FTIR and SEM. The ε-CL monomer was intercalated and dispersed into the layered structure of OREC, and the PCL/OREC nanocomposites were successfully synthesized by *in situ* intercalation polymerization. The yield and molecular weight of PCL/OREC were investigated
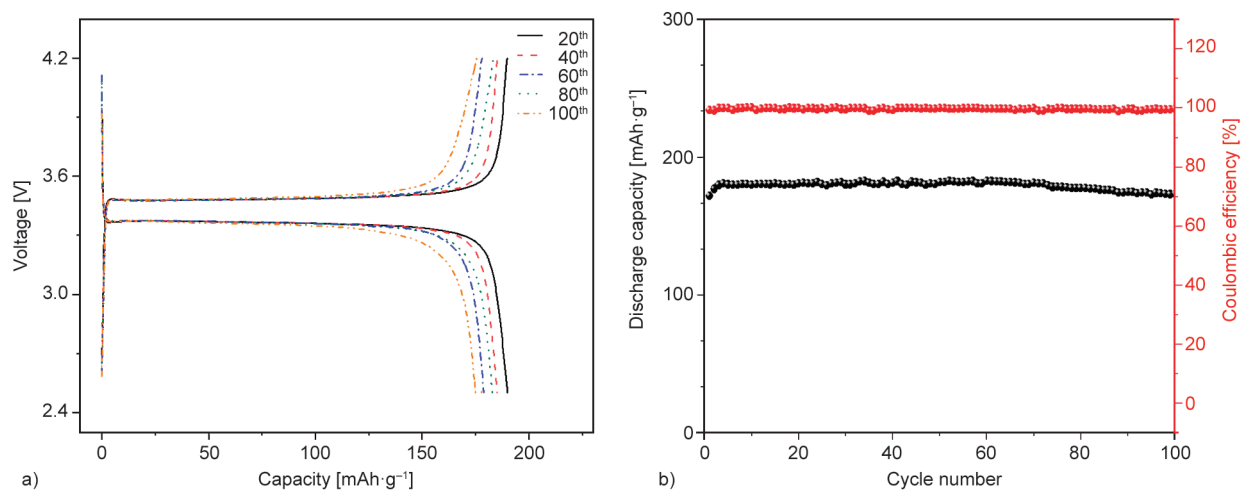
Figure 13. a) Charge and discharge profiles and b) cycle performance of CPEs (PCL/OREC) in LiFePO$_4$/CPEs/Li-battery.

by orthogonal experiment, and the best formula was obtained. The XRD and SEM micrographs show that OREC exists in a stripped state in PCL matrix with good dispersion. By TG and DSC tests, it was found that the addition of OREC made PCL have higher thermal stability and lower crystallinity. Moreover, through DMA analysis, PCL/OREC has higher energy storage modulus and stronger molecular chain motion ability compared with pure PCL. In addition, PCL/OREC has strong electrical conductivity at higher temperatures and exhibits enhanced cyclic stability. We expect that the synthesis of PCL/OREC nanocomposites by *in situ* intercalation polymerization not only provides a reliable method for PCL-based nanocomposites, but also provides a wider application prospect for PCL materials.

Acknowledgements

References

[1] Vertuccio L., Gorrasi G., Sorrentino A., Vittoria V.: Nano clay reinforced PCL/starch blends obtained by high energy ball milling. Carbohydrate Polymers, **75**, 172–179 (2009).
https://doi.org/10.1016/j.carbpol.2008.07.020

[2] Ye W., Zaheer M., Li L., Wang J., Xu H., Wang C., Deng Y.: Hyperbranched PCL/PS copolymer-based solid polymer electrolytes enable long cycle life of lithium metal batteries. Journal of the Electrochemical Society, **167**, 110532 (2020).
https://doi.org/10.1149/1945-7111/aba3fd

[3] Woo H. J., Majid S. R., Arof A. K.: Transference number and structural analysis of proton conducting polymer electrolyte based on poly(ε-caprolactone). Materials Research Innovations, **15**, 49–54 (2013).
https://doi.org/10.1179/143307511x13031890747697

[4] Fonseca C. P., Rosa D. S., Gaboardi F., Neves S.: Development of a biodegradable polymer electrolyte for rechargeable batteries. Journal of Power Sources, **155**, 381–384 (2006).
https://doi.org/10.1016/j.jpowsour.2005.05.004

[5] Eriksson T., Mindemark J., Yue M., Brandell D.: Effects of nanoparticle addition to poly(ε-caprolactone) electrolytes: Crystallinity, conductivity and ambient temperature battery cycling. Electrochimica Acta, **300**, 489–496 (2019).
https://doi.org/10.1016/j.electacta.2019.01.117

[6] Bhagabati P., Chaki T. K., Khastgir D.: Panoptically exfoliated morphology of chlorinated polyethylene (CPE)/ethylene methacrylate copolymer (EMA)/layered silicate nanocomposites by novel *in situ* covalent modification using poly(ε-caprolactone). RSC Advances, **5**, 38209–38222 (2015).
https://doi.org/10.1039/c4ra15723k

[7] Wan C., Qiao X., Zhang Y., Zhang Y.: Effect of different clay treatment on morphology and mechanical properties of PVC-clay nanocomposites. Polymer Testing, **22**, 453–461 (2003).
https://doi.org/10.1016/s0142-9418(02)00126-5

[8] Ilsouk M., Raihane M., Lahcini M., Meri R. M., Zicāns J., Cimdina L. B., Kharas G. B.: Bionanocomposites poly(ε-caprolactone)/organomodified Moroccan beidellite clay prepared by *in situ* ring opening polymerization: Characterizations and properties. Journal of Macromolecular Science Part A: Pure and Applied Chemistry, **54**, 201–210 (2017).
https://doi.org/10.1080/10601325.2017.1282229

[9] Nabgui A., El Assimi T., El Meziane A., Luinstra G. A., Raihane M., Gouhier G., Thébault P., Draoui K., Lahcini M.: Synthesis and antibacterial behavior of bio-composite materials-based on poly(ε-caprolactone)/bentonite. European Polymer Journal, **156**, 110602 (2021).
https://doi.org/10.1016/j.eurpolymj.2021.110602

[10] Wu T-M., Wu C-Y.: Biodegradable poly(lactic acid)/chitosan-modified montmorillonite nanocomposites: Preparation and characterization. Polymer Degradation and Stability, **91**, 2198–2204 (2006).
https://doi.org/10.1016/j.polymdegradstab.2006.01.004

[11] Kotal M., Bhowmick A. K.: Polymer nanocomposites from modified clays: Recent advances and challenges. Progress in Polymer Science, **51**, 127–187 (2015).
https://doi.org/10.1016/j.progpolymsci.2015.10.001

[12] Gain O., Espuche E., Pollet E., Alexandre M., Dubois P.: Gas barrier properties of poly(ε-caprolactone)/clay nanocomposites: Influence of the morphology and polymer/clay interactions. Journal of Polymer Science Part B: Polymer Physics, **43**, 205–214 (2005).
https://doi.org/10.1002/polb.20316

[13] Shen Y., Yu X., Wang Y.: Facile synthesis of modified rectorite (M-REC) for effective removal of anionic dye from water. Journal of Molecular Liquids, **278**, 12–18 (2019).
https://doi.org/10.1016/j.molliq.2019.01.045

[14] Yang H., Weijun L., Weiqing W., Qiming F., Jing L.: Synthesis of a carbon@rectorite nanocomposite adsorbent by a hydrothermal carbonization process and their application in the removal of methylene blue and neutral red from aqueous solutions. Desalination and Water Treatment, **57**, 13573–13585 (2015).
https://doi.org/10.1080/19443994.2015.1074120

[15] Zhang H., Zhu C., Yan K., Yu J.: Effect of rectorite and its organic modification on properties of bitumen. Journal of Materials in Civil Engineering, **27**, C4014002 (2015).
https://doi.org/10.1061/(ASCE)MT.1943-5533.0000972

[16] Yuan L., Gu A., Liang G., Ma X., Lin C., Chen F.: Properties and structures of novel cyanate ester/organic rectorite nanocomposites. Polymer Engineering and Science, **52**, 2443–2453 (2012).
https://doi.org/10.1002/pen.23198

[17] Wang L., Wang Y-Q., Zhang L-Q., Wu Y-P.: Rectorite powder modified by butadiene-styrene-vinyl pyridine rubber: Structure and its dispersion in styrene-butadiene rubber. Journal of Applied Polymer Science, **127**, 765–771 (2013).
https://doi.org/10.1002/app.37781

[18] Szeluga U., Kumanek B., Trzebicka B.: Synergy in hybrid polymer/nanocarbon composites. A review. Composites Part A: Applied Science and Manufacturing, **73**, 204–231 (2015).
https://doi.org/10.1016/j.compositesa.2015.02.021

[19] Chen H., Yang H., Xi Y.: Highly ordered and hexagonal mesoporous silica materials with large specific surface from natural rectorite mineral. Microporous and Mesoporous Materials, **279**, 53–60 (2019).
https://doi.org/10.1016/j.micromeso.2018.12.014

[20] Du C., Yang H.: Investigation of the physicochemical aspects from natural kaolin to Al-MCM-41 mesoporous materials. Journal of Colloid Interface Science, **369**, 216–222 (2012).
https://doi.org/10.1016/j.jcis.2011.12.041

[21] Wang W., Wang A.: Preparation, characterization and properties of superabsorbent nanocomposites based on natural guar gum and modified rectorite. Carbohydrate Polymers, **77**, 891–897 (2009).
https://doi.org/10.1016/j.carbpol.2009.03.012

[22] Angaji M. T., Zinali A. Z., Qazvini N. T.: Study of physical, chemical and morphological alterations of smectite clay upon activation and functionalization *via* the acid treatment. World Journal of Nano Science and Engineering, **3**, 161–168 (2013).
https://doi.org/10.4236/wjnse.2013.34019

[23] Du C., Yang H.: Simple synthesis and characterization of nanoporous materials from talc. Clays and Clay Minerals, **57**, 290–301 (2009).
https://doi.org/10.1346/ccmn.2009.0570302

[24] Zhang R., Zheng P., Ma X.: Preparation and catalytic properties of magnetic rectorite-chitosan-Au composites. Journal of Alloys and Compounds, **690**, 381–389 (2017).
https://doi.org/10.1016/j.jallcom.2016.08.131

[25] Huang M., Tu H., Chen J., Liu R., Liang Z., Jiang L., Shi X., Du Y., Deng H.: Chitosan-rectorite nanospheres embedded aminated polyacrylonitrile nanofibers *via* shoulder-to-shoulder electrospinning and electrospraying for enhanced heavy metal removal. Applied Surface Science, **437**, 294–303 (2018).
https://doi.org/10.1016/j.apsusc.2017.12.150

[26] Yang H., Deng Y., Du C., Jin S.: Novel synthesis of ordered mesoporous materials Al-MCM-41 from bentonite. Applied Clay Science, **47**, 351–355 (2010).
https://doi.org/10.1016/j.clay.2009.11.050

[27] Megherbi R., Mrah L., Marref M.: Maghnite: An innovative inorganic reinforcement used in the synthesis of polystyrene nanocomposites with optimized thermal and mechanical properties. Iranian Polymer Journal, **31**, 223–236 (2021).
https://doi.org/10.1007/s13726-021-00995-w

[28] Sun Z., Park Y., Zheng S., Ayoko G. A., Frost R. L.: Thermal stability and hot-stage Raman spectroscopic study of Ca-montmorillonite modified with different surfactants: A comparative study. Thermochimica Acta, **569**, 151–160 (2013).
https://doi.org/10.1016/j.tca.2013.07.022

[29] Liao L. Q., Liu L. J., Zhang C., He F., Zhuo R. X., Wan K.: Microwave-assisted ring-opening polymerization of ε-caprolactone. Journal of Polymer Science Part A: Polymer Chemistry, **40**, 1749–1755 (2002).
https://doi.org/10.1002/pola.10256

[30] Lepoittevin B., Pantoustier N., Devalckenaere M., Alexandre M., Kubies D., Calberg C., Jérôme R., Dubois P.: Poly(ε-caprolactone)/clay nanocomposites by *in situ* intercalative polymerization catalyzed by dibutyltin dimethoxide. Macromolecules, **35**, 8385–8390 (2002).
https://doi.org/10.1021/ma020300w

[31] Yang G., Ma R., Zhang S., Liu Z., Pei D., Jin H., Liu J., Du W.: Microwave-assisted *in situ* ring-opening polymerization of ε-caprolactone in the presence of modified halloysite nanotubes loaded with stannous chloride. RSC Advances, **12**, 1628–1637 (2022).
https://doi.org/10.1039/d1ra07469e

[32] Di Maio E., Iannace S., Sorrentino L., Nicolais L.: Isothermal crystallization in PCL/clay nanocomposites investigated with thermal and rheometric methods. Polymer, **45**, 8893–8900 (2004).
https://doi.org/10.1016/j.polymer.2004.10.037

[33] Yeh J-M., Yao C-T., Hsieh C-F., Lin L-H., Chen P-L., Wu J-C., Yang H-C., Wu C-P.: Preparation, characterization and electrochemical corrosion studies on environmentally friendly waterborne polyurethane/Na^+-MMT clay nanocomposite coatings. European Polymer Journal, **44**, 3046–3056 (2008).
https://doi.org/10.1016/j.eurpolymj.2008.05.037

[34] Omori S., Matsushita M., Kato F., Ohki Y.: Effect of crystallinity on electrical conduction characteristics of poly(l-lactic acid). Japanese Journal of Applied Physics, **46**, 3501–3503 (2007).
https://doi.org/10.1143/jjap.46.3501

[35] Deng X., Liu F., Luo Y., Chen Y., Jia D.: Preparation, characterization and application of polymeric diols with comb-branched structure and their nanocomposites containing montmorillonites. European Polymer Journal, **43**, 704–714 (2007).
https://doi.org/10.1016/j.eurpolymj.2006.12.003

[36] Li Z., Fu J., Zhou X., Gui S., Wei L., Yang H., Li H., Guo X.: Ionic conduction in polymer-based solid electrolytes. Advanced Science, **10**, 2201718 (2023).
https://doi.org/10.1002/advs.202201718

[37] Zhou Y-K., He B-L., Zhou W-J., Huang J., Li X-H., Wu B., Li H-L.: Electrochemical capacitance of well-coated single-walled carbon nanotube with polyaniline composites. Electrochimica Acta, **49**, 257–262 (2004).
https://doi.org/10.1016/j.electacta.2003.08.007

[38] Pagacz J., Pielichowski K.: PVC/MMT nanocomposites. Journal of Thermal Analysis and Calorimetry, **111**, 1571–1575 (2012).
https://doi.org/10.1007/s10973-012-2484-2

[39] Zhang R., He X., Lai Z., Yang D.: Effect of some inorganic particles on the softening dispersion of the dynamics of butyl rubber. Polymer Bulletin, **74**, 1031–1043 (2016).
https://doi.org/10.1007/s00289-016-1761-9

[40] Yeh J-M., Kuo T-H., Huang H-J., Chang K-C., Chang M-Y., Yang J-C.: Preparation and characterization of poly(o-methoxyaniline)/Na$^+$-MMT clay nanocomposite *via* emulsion polymerization: Electrochemical studies of corrosion protection. European Polymer Journal, **43**, 1624–1634 (2007).
https://doi.org/10.1016/j.eurpolymj.2007.01.040

[41] Wang J., Yu X., Wang C., Xiang K., Deng M., Yin H.: PAMPS/MMT composite hydrogel electrolyte for solid-state supercapacitors. Journal of Alloys and Compounds, **709**, 596–601 (2017).
https://doi.org/10.1016/j.jallcom.2017.03.157

[42] Lu Y., Li L., Zhang Q., Niu Z., Chen J.: Electrolyte and interface engineering for solid-state sodium batteries. Joule, **2**, 1747–1770 (2018).
https://doi.org/10.1016/j.joule.2018.07.028

[43] Chen R., Qu W., Guo X., Li L., Wu F.: The pursuit of solid-state electrolytes for lithium batteries: From comprehensive insight to emerging horizons. Materials Horizons, **3**, 487–516 (2016).
https://doi.org/10.1039/c6mh00218h